Trabajo Fin de Máster

Nanoestructuras 3D para la siguiente generación de memorias MRAM

3D Nanostructures for the next generation of MRAM Memories

Author

Omar Karam Mounsif

Directors

Alberto Anadón Barcelona

Cristina Bran

Faculty of Science
2025

Acknowledgements

Bismillah. I want to first dedicate the biggest words of gratitude to my mother, Rachida, my brother Reda and my father, Jamal. You have always inspired me and pushed me beyond limits I thought I would never surpass, always driven by a light that I think you could see in me from long ago before I started noticing it myself. You are my greatest treasure.

To Alberto Anadón and Cristina Bran, or as I refer to them when talking to my friends, ”my science parents”. Thank you for putting the trust and the work that is necessary to teach a beginner. I really hope other students have the privilege of learning from you, and I surely wish that our paths cross again ahead. I have always dreamt of pursuing a career as a scientist, and working with you has really cemented the belief that this is the path I want to follow going onwards. I would also like to thank Prof. Amalio Fernández-Pacheco and Dr. Pablo Olleros for their contributions, their support and their insight, for including me and giving me the opportunity to have a first-hand experience on how research is done.

Now, this part is dedicated to my friends. I know I have been missing for a very long time, but what you are now reading is part of the reason behind it. I know you all know how important this is to me, and I want to thank you for your understanding, for letting me be and for being there in times of need. Thank you for being the way you are, for always bringing joy into my life, and for always giving me reasons to admire you and be proud. To Leyre as well, a friend I have met only this year. Sharing our work progress almost every week has been of great help to keep going forward. I have really high hopes for your career and I know for a fact it won't be long before I start seeing your name in bold fonts everywhere.

Some special mentions to finish: Nikols Mora, a very dear friend of mine, a brother even, without whom I would have never had the opportunity to finish this degree. This one is for you, especially. I have not wasted nor the gift, nor the time. Finally, to a man who has been like a grandfather (and a friend) to me, Don Ramón Nieto. A man that has recently left us to join my uncle, Alfredo. I may not be your blood's grandson, but you and your family have always made me feel like home. I know both of you watch us and care for us from up there, surely going around in lots of hikes together, like back when you used to hang out down here with us.

I am grateful for having such a long list of reasons and people that I feel thankful for. So long that a whole page falls short. My biggest wish after this is just that I keep getting opportunities to make my dreams come true, and pages where to express my gratitude for it. **Alhamdulillah**.

Abstract

Skyrmion nucleation and motion are at the core of the development of new technologies such as racetrack memories or new-gen MRAMs, which feature larger storage capacities and faster and more efficient operations. The objective of this project is to take the first steps in design and development of 3D nanostructures capable of hosting Skyrmions to investigate their nucleation and motion driven by thermal gradients. Manipulating Skyrmions using thermal effects offers several advantages over electrical methods, as it avoids complications such as the Skyrmion Hall effect, which can disrupt stable trajectories. Additionally, using thermal gradients can lead to lower energy consumption, making this approach more efficient and sustainable for future spintronic applications. For this purpose, a series of thermal and micromagnetic simulations are carried out using the COMSOL and MuMAX3 softwares to gain knowledge about the thermal gradients that appear in different structures and predict more reliably how these could affect the movement of Skyrmions. The modeling is complemented by experimental characterization of the magnetic state of the fabricated nanostructures, showing hystesis loops compatible with the appearance of Skyrmions.

La nucleación y el movimiento de los Skyrmions están en el centro del desarrollo de nuevas tecnologías como las memorias de tipo "racetrack" o las MRAMs de nueva generación, que presentan mayores capacidades de almacenamiento y operaciones más rápidas y eficientes. El objetivo de este proyecto es dar los primeros pasos para el diseño y desarrollo de nanoestructuras 3D capaces de alojar Skyrmions e investigar su nucleación y movimiento impulsado por gradientes térmicos. Manipular Skyrmions usando efectos térmicos ofrece varias ventajas sobre los métodos eléctricos, ya que evita complicaciones como el efecto Hall de Skyrmions, que puede dificultar trayectorias estables. Además, el uso de gradientes térmicos puede conducir a un menor consumo de energía, haciendo que este enfoque sea más eficiente y sostenible para futuras aplicaciones espintrónicas. Con este propósito, se llevan a cabo una serie de simulaciones térmicas y micromagnéticas usando los softwares COMSOL y MuMAX3 para obtener conocimiento sobre los gradientes térmicos que aparecen en diferentes estructuras y cómo estos afectan el movimiento de los Skyrmions. El modelado se complementa con la caracterización experimental del estado magnético de las nanoestructuras fabricadas, obteniendo ciclos de histéresis compatibles con la aparición de Skyrmions.

Index

Chapter 1

Introduction

State of the art

In recent times, energy consumption associated with the processing and storage of data has increased drastically and predictions state that it will keep on doing so as device performance and specification demands grow [1, 2, 3]. This growing energy demand has inspired the exploration of alternative technologies aimed at reducing power consumption. The development of low-power, non-volatile magnetic memory technologies [4] may produce a solution capable of bridging the gap between concepts and large-scale applications.

Skyrmion-based racetrack memories have emerged as a promising alternative for this. Skyrmions —topologically protected magnetic nanoscale quasiparticles —offer great robustness against defects and external perturbations when compared to conventional magnetic domain structures [5, 6, 7]. Their size, topological protection and low depinning currents make them suitable candidates for high-density, energy-efficient memory and logic devices.

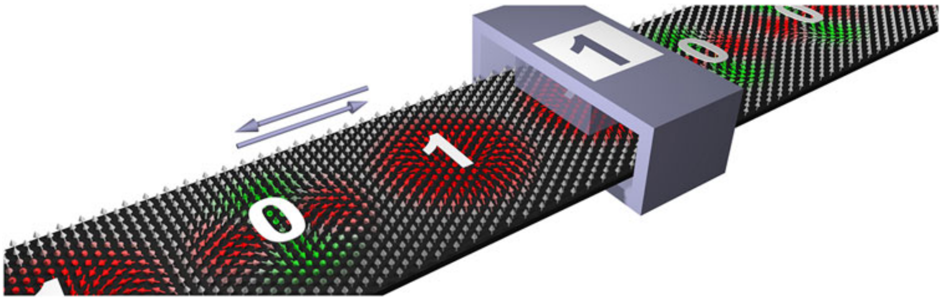

Figure 1.1: Schematic representation of a racetrack memory. (*Hoffmann et. al.*)[5]

Figure (1.1) depicts the mechanism of a Skyrmion-based racetrack memory. A detector is placed and reads the magnetic state of each one and assigns a 1 or a 0 (bit information) depending on the direction of the measured magnetic moment, m_z of each Skyrmion. This would allow us to read and write using them as carriers of digital bit information. However, the entire process relies heavily on the ability to reliably move the Skyrmions.

The topic of Skyrmion motion has been widely addressed, unraveling a series of issues that need to be overcome to achieve controlled movement. For example, when driven by electrical currents, Skyrmions bend their trajectories due to the Skyrmion Hall effect, limiting reliable device operation [8, 9, 10]. Alternative driving mechanisms have been proposed to tackle the problem of controlled motion —such as thermal and magnetic property gradients—but their precise influence on Skyrmion dynamics is not yet fully understood [11, 12, 13, 14].

Recent advances in skyrmion research have significantly deepened our understanding of Skyrmion thermal motion and potential for novel device applications such as unconventional computing[15], where they demonstrated that thermal fluctuations can induce Brownian diffusion of Skyrmions in low-pinning multilayers. Theoretical background to the fundaments behind these effects is also being developed[16] by systematically studying temperature-gradient-driven Skyrmion motion in single-layer ferromagnets and multilayers. Entropic torques, thermally generated spin-currents and magnonicand torques compete and the resulting motion direction thus depends on material parameters. Notably, Skyrmions move toward hot regions in single layers but toward cold regions in multilayers according to this study. Regardless, a complete experimental validation is still missing. Existing studies provide insight into Skyrmion nucleation and motion in planar (2D) structures [8, 17, 18, 19], but their behavior in three-dimensional ones remains largely unexplored, especially in regards to how thermal effects will influence their dynamics and stability in these systems. 3D systems are particularly interesting in this topic, since they allow for much higher thermal gradients, opening new possibilities to explore these rich phenomena.

Skyrmions

A Skyrmion is a topological defect in the magnetization texture consisting in local whirls of the spins in a magnetic material. Their utility comes from their particle-like behavior, as they can be moved, created and annihilated. The fact that they also have an overall collective magnetic moment (m_z) makes them a suitable candidate for applications in novel digital storage devices such as racetrack memories [20]. However, as mentioned previously, there are still gaps to fill when it comes to an understanding that would allow us to integrate them as a reliable mechanism that can be used and reproduced at a large scale.

Ferromagnets, seen from the magnetic spins' perspective, tend to form ordered configurations, as they constitute energy-minimizing states. In a magnetic system with an out-of-plane anisotropy, the typical magnetic configurations are those in which all spins align uniformly (either pointing up or down). In certain conditions, depending on the internal interactions and external influences, non-trivial spatial arrangements can emerge.

For example, during the transition between ”all up” and ”all down”, the so-called reversal of the magnetization, the spin population in a magnetic material can break into domains. These domains are regions in which the spins point in a specific direction, different from neighboring ones.

Skyrmions, named after Tony Skyrme, who proposed their theoretical existence[21], constitute one of these nontrivial configurations. These structures arise due a special interaction, known as Dzyaloshinskii-Moriya interaction (DMI) [7]. DMI describes an energy component in the overall Hamiltonian of the system that stems from the interaction between two magnetic spins that are spatially close to a heavy atom with strong spin-orbit coupling, and it favors a non-collinear alignment of neighboring spins [22], playing a central role in the stabilization of these domains. This interaction's Hamiltonian is described as:

$$H_{DMI} = -D_{12}(S_1 \times S_2) \tag{1.1}$$

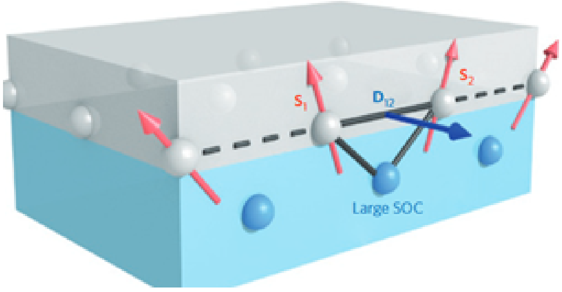

Figure 1.2: Visualization of interfacial DMI, with a ferromagnetic layer (grey) on top a heavy atom layer (blue). (*A. Fert et. al.*)[7]

As any magnetic texture, Skyrmions are found in magnetic materials, but the necessary setup for their emergence consists in more than just a magnetic film. The usual arrangement is done by stacking a trilayer composed of // Heavy metal / Ferromagnet with out of plane magnetic anisotropy / Isolating layer // (i.e. Pt/Co/MgO). The first two layers are critical, as they constitute the basic requirements for the DMI to take place. The third one acts as an isolating agent against oxidation, although it also serves the purpose of creating a non-symmetric layer distribution, as DMIs arise only in systems lacking inversion symmetry [22]. Different combinations of these layers and multiple repetitions can modify the properties of the system (i.e. anisotropy, stacking order, dipolar interaction, etc.) and provide an avenue to tune the properties of the Skyrmions[23].

Skyrmion morphology varies depending on the system's properties and conditions it is subjected to, but without taking size into account, we can distinguish two main types differentiated by how the spins are oriented within this domain and, more importantly, how they rotate as their position reaches the wall. We therefore categorize the walls (and subsequently, Skyrmions as well) as Néel or Bloch. In Néel configurations, the spins' rotation axis is perpendicular to the surface vector of the wall. In Bloch Skyrmions, the rotation vector is parallel to the wall's surface vector (Fig. 1.3). Thin layering configurations (like the one shown in Fig. (1.2)) favor energetically Néel Skyrmions (Fig. 1.4b) rather than Bloch Skyrmions (Fig. 1.4a), that are more common in systems where instead of thin magnetic layers, there is bulk material [24].

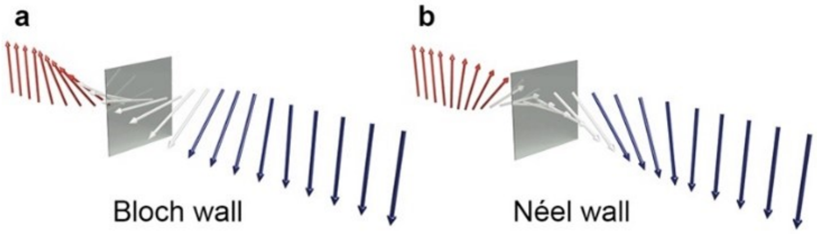

Figure 1.3: Visualization of domain walls.

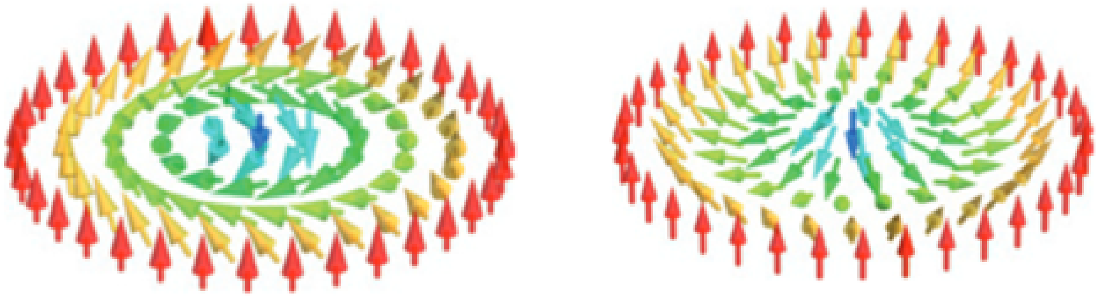
(a)
(b)

Figure 1.4: Types of Skyrmions. (a) shows a Bloch Skyrmion, whereas (b) shows a Néel type Skyrmion. (*A. Fert et. al.*)[7]

This master's thesis

This work contains the preliminary steps to the experimental phase of a project dedicated to the understanding of Skyrmion-related phenomena. We aim to shed some light on the question of the influence of thermal effects in Skyrmions by investigating their behavior in nanofabricated 3D devices. The strategy to achieve this consists of generating local temperature gradients in the order of $\nabla T \sim$ 10s or 100s of K/μm. These gradients are greater than the ones obtained in 2D systems, where they are found to be in the range of $\nabla T \sim 1K/\mu m$ [17]. This will ultimately allow for a deeper understanding on how thermal driving and dimensionality affect nucleation, stability and motion.

This master thesis comprises the results of a series of finite element simulations that generated the thermal (and field) gradients subsequently used in the micromagnetic simulations to study the Skyrmion motion. It also includes details of the fabrication process of the studied structures, as well as the characterization methods used.

Chapter 2

COMSOL Thermal simulations

In this chapter we will study the thermal profiles of different Skyrmion racetracks. We aim to find an optimal geometry to maximize the thermal gradients while minimizing other spurious contributions such as the Oersted field. The complexity of the configurations involved limits the use of analytical results and requires specialized tools such as finite differences calculations. In our case, we have used COMSOL multiphysics for this purpose. In particular, we will experimentally explore two distinct systems: 2D microdevices and 3D nanodevices. In the case of the 2D devices, the heat is always produced by an electrical heater whereas in the 3D nanodevices it is provided by a laser. In all the cases, we will study the thermal profiles and then, for the 2D devices, we will also look at the Oersted field distribution generated by the current injected in the heater. This will be critical for the design of optimal devices using both micromagnetic simulations and experiments.

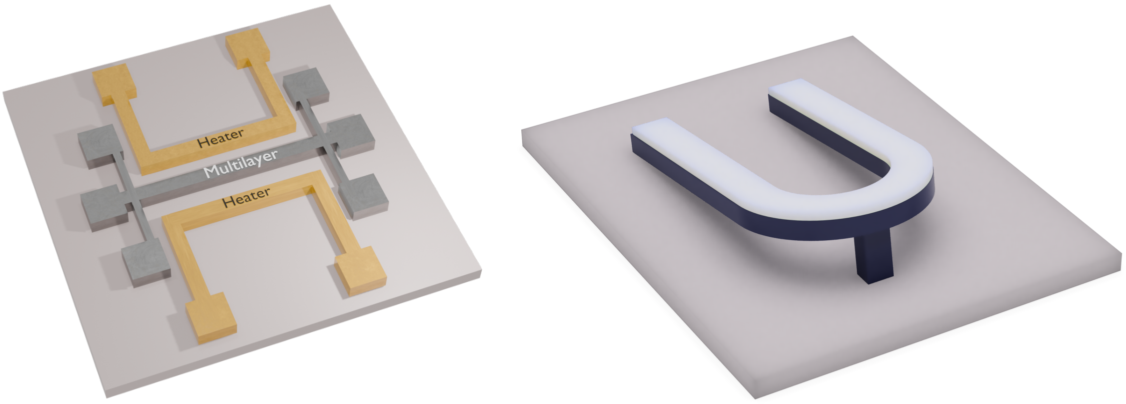

(a) (b)

Figure 2.1: (a) 2D microdevice for nucleation and motion of Skyrmions. Adapted from [17]. (b) 3D structure

2.1 Finite differences calculations in 2D and 3D geometries

2.1.1 2D microdevices

An example of a 2D device is shown in figure 2.1a. In this device, the active bar with the magnetic stack is placed between two metallic heaters providing the option to change the directionality of the temperature gradient by using one heater or the other.

This setup is designed for different transport and thermal transport measurements. It is possible to perform longitudinal and transversal (Hall) resistivity measurements with four probes to avoid contact contributions to resistivity, allowing to measure changes in the magnetization produced by the existence of magnetic domains. It is also possible to use the heaters in combination to observe how the Hall resistivity is affected by these domains, since it is proportional to the z-component of the magnetization[25]. Similarly, it also allows to perform thermo-magnetic measurements, such as the Nernst effect, using the two heaters to produce a thermal gradient and the different electrical contacts to measure the thermo-spin voltage (see figure 2.1a). An electrical current is passed through one of the heaters to generate a thermal gradient and subsequently, the combination of heat flow and magnetic field leads to the generation of a voltage perpendicular to both[26].

In this work, we compare two devices with different heater geometries and then estimate the temperature and Oersted field profiles. Our goal is to create a platform to study nucleation and motion of Skyrmions in planar structures by finding the optimal conditions of operation by maximizing the temperature gradient as much as possible while minimizing the Oersted field building on previous studies in similar systems[17]. For this, we model two different gold conductor geometries of section (2 x 0.05 μm^2) on top of a SiO_2 ($0.09 \mu m$) + crystalline Si ($9.91 \mu m$) substrate in order to have the closest possible system to the real devices that we will show later in this manuscript. A current of 0.161A is passed through the conductors and the heating of the surrounding area takes place by Joule effect.

Temperature profiles

Fig.(2.2) shows the temperature distribution at the substrate's surface and Fig.(2.3) shows the temperature profiles at the line cuts showed as dashed lines in figure 2.2. In the final devices, the multilayer sample will be placed at $1 \mu m$ distance from the heat source. The active bar's width is around $10 \mu m$. Due to the higher thermal gradient, the nucleation occurs at the region of the active bar closest to the heater and thus we

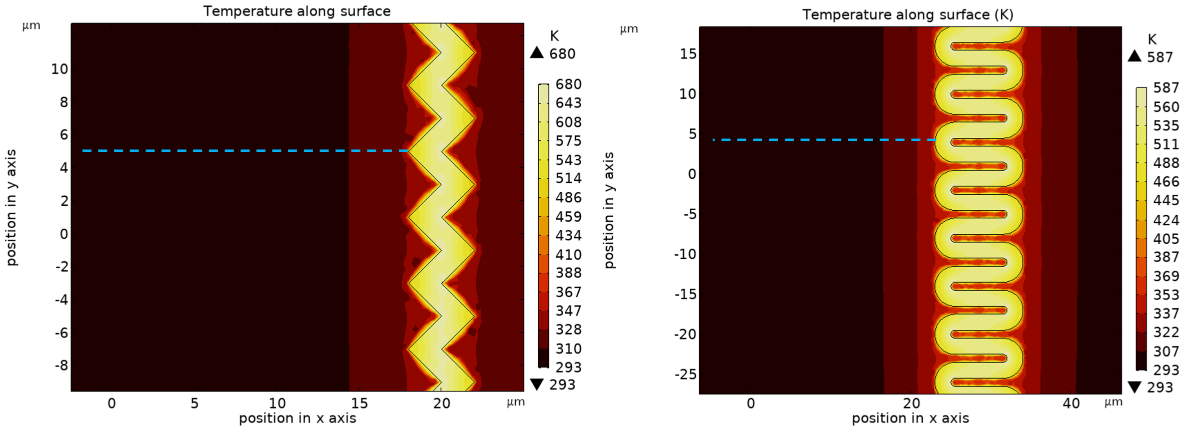

(a) (b)

Figure 2.2: Temperature distribution along surface for two conductor geometries, zigzag (ZZC) (a) and sinusoidal (SNC) (b).

define a region of interest (ROI) of the first 2 μm of the bar. The resulting temperature gradients for such region are shown in Fig.(2.3).

In the ROI the temperature gradient is in the order of -5 K/μm for ZZC (Fig. 2.3c) and -6 K/μm for SSC (Fig. 2.3d). This is consistent with the reported values from Wang et al. [17] of 1-3 K/μm. The slight differences appear due to slight changes in the material, geometry and applied current used. The higher thermal gradient obtained for the SSC device is a good indication of an improvement over the ZZC geometry.

Oersted Field distribution

Oersted field is generated by electric currents and is highly dependent on the geometry and density of the electric current. The interaction between Skyrmions and the Oersted field is a very active topic[27] since it offers a versatile mechanism for Skyrmion manipulation without the need for direct current injection into the magnetic layer, reducing Joule heating in the sample and preserving Skyrmion stability. Previous studies have demonstrated that Oersted field can efficiently control Skyrmion size [28, 29], and motion [30]. **Since we aim to study the effect of thermal gradients in Skyrmions, we need to minimize the Oersted field**, as well as know their values to account for them in future estimations[17]. The current density distribution is different for the two selected geometries for the conductors in 2D microdevices, as shown in Fig. (2.4) and thus the Oersted field generated (see figure 2.5).

Local changes in current densities contribute to the overall field distributed along the surface. We have used the current profiles to calculate the corresponding magnetic

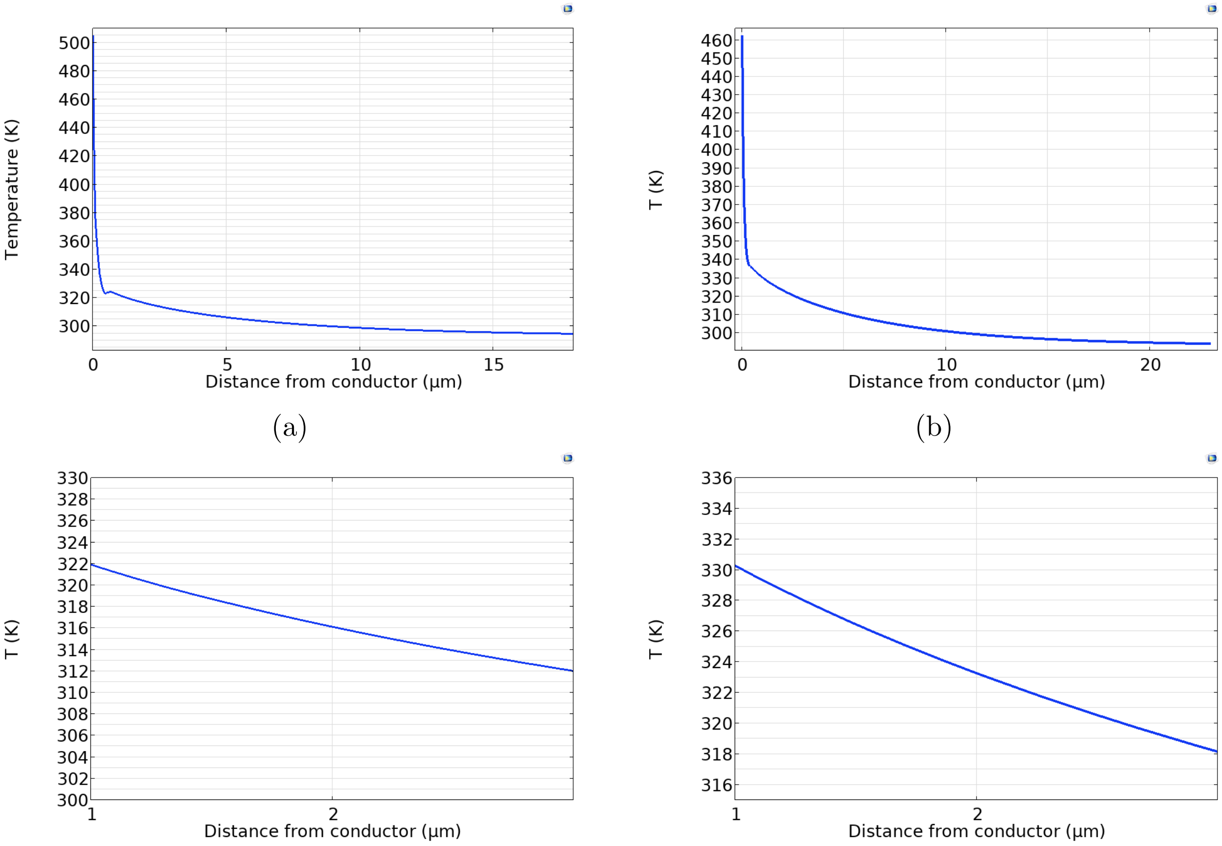

(a) (b)

(c) (d)

Figure 2.3: Temperature values with respect to the distance from the conductors, with the zero positioned at its edge, where (a) and (b) show the values obtained for each of the drawn lines in Fig. 2.2a ZZC and Fig.(2.2b) SSC, respectively. Graphs in (c) and (d) correspond to the ROI in both systems (a-c;b-d), that is between 1 - 3 μm away from the conductor's boundaries in both cases.

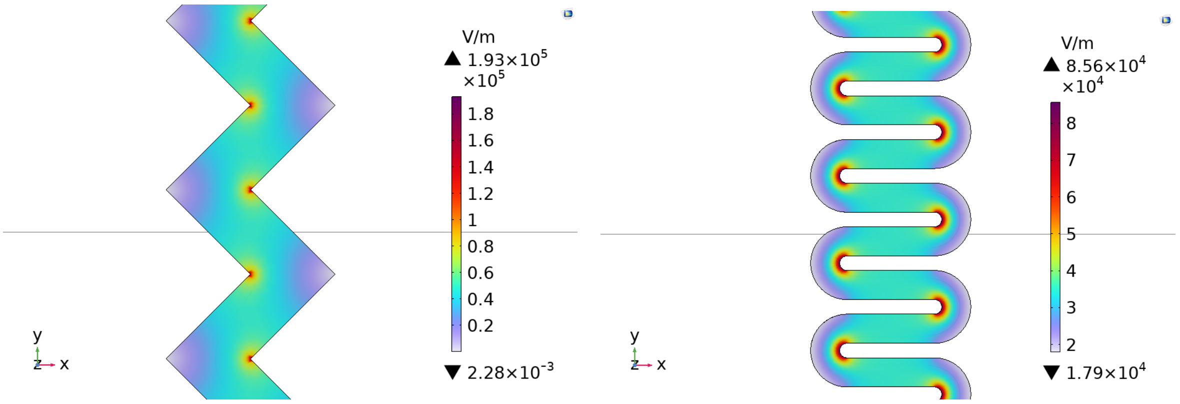

(a) (b)

Figure 2.4: Electric field norm distributions along each conductor, in V/m ZZC (a) and sinusoidal SNC (b). Higher values of this norm indicate higher charge concentrations, pointing an uneven distribution of electric charge in the system.

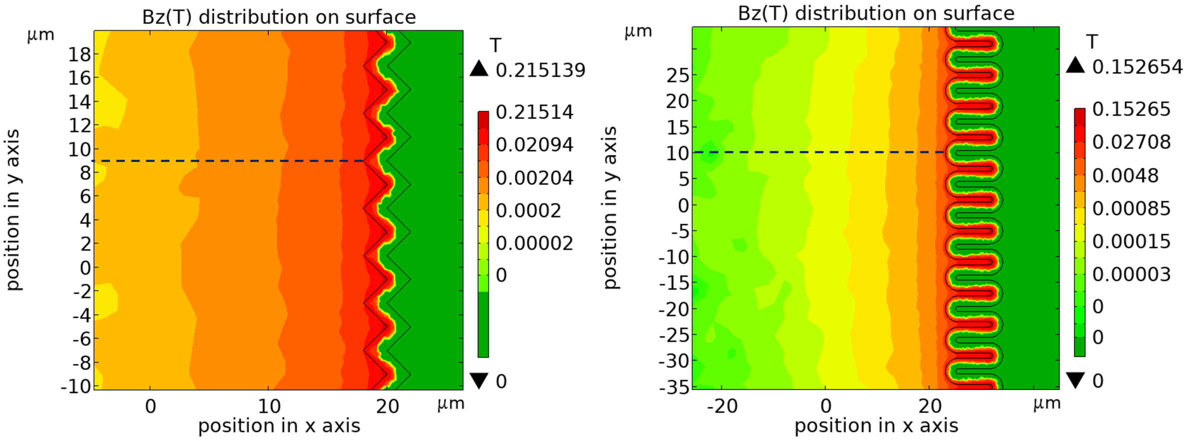

(a) (b)

Figure 2.5: Oersted field distribution in the z direction (Out of plane) for each setup along the surface. (a) ZZC, (b) SSC. Color scaling is in logarithmic scale for contrast purposes. For that reason the right side of each conductor does not display values, as the field in this region is Bz<0.

fields and gradients that will be used later to analyze their influence on motion and stability.

The same way we plotted temperature along a line perpendicular to the y axis in the region of interest, a measurement of equal characteristics has been performed to gain a clear picture of the Oersted field variation in the ROI (Fig. 2.6), complementary to the information shown in Fig. (2.5).

By looking at Figs. (2.6c; 2.6d) we can estimate that there is a magnetic field gradient of about $\nabla B = -0.002$ T$/\mu m$ for both systems' ROIs. This, in the end makes it easier to choose a conductor geometry for an experimental setup as the objective of this field's analysis is to determine which configuration would minimize this component. Having a similar gradient for both, we pay attention at the maximum and minimum field values and we can see that, as the ZZC (Fig. 2.6c) has a maximum of 8.5 mT and a minimum of 4.5 mT, the SSC (Fig. 2.6d) shows a maximum of 7.5 mT and a minimum of 3.5 mT. In conclusion, the sinusoidal conductor geometry SSC yields a lower Oersted field, although the gradient would be similar as in the other case.

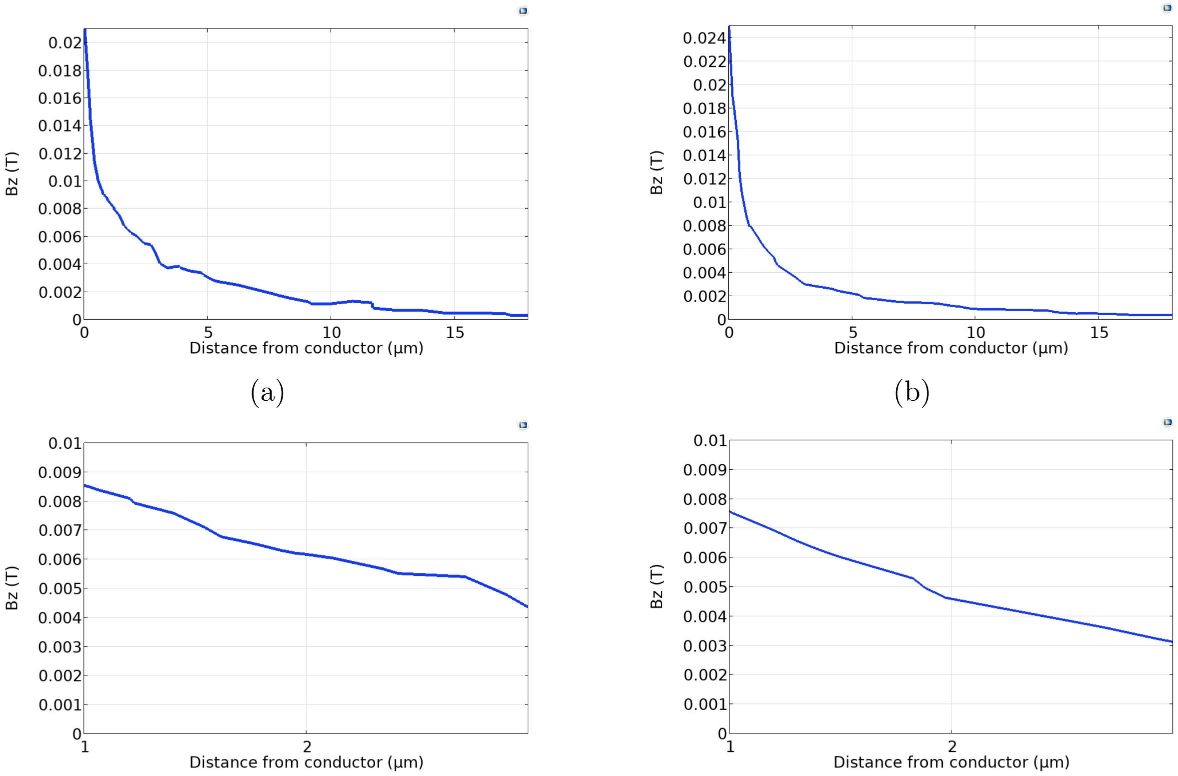

(a) (b)

(c) (d)

Figure 2.6: Oersted field distributions along dotted lines in Figure 2.5. (a) corresponds to the ZZC system and (b) to the SSC one. The (c-a) and (d-b) graphs represent the field distribution in the whole region, as well as their respective ROIs.

2.1.2 3D device simulation

We now move to the second main system, 3D nanostructures. In these structures it is possible to gain larger temperature gradients than the ones expected in 2D as heat flow is more confined and has fewer available dissipation paths. Here, heating will be done using an optical source due to the complexity of fabricating electrical devices in 3D nanostructures. We use similarly COMSOL heat transfer package, implementing the geometry of the nanostructures itself and using the thermal conductivity of platinum [31, 32]. We use realistic values for continuous laser beam of a power of 3 mW focused with a 10x objective into a beam width with 10 μm of diameter we obtain a fluence of $3.8{\cdot}10^7$ W/m^2. We can simulate the input heat flux in the surface considering an absorption of the TaOx surface of the multilayer of about 88%[33]. In this case, we will only obtain the temperature gradient distribution along the structure, as we don't expect a magnetic field distribution along our sample. The desired structure is showcased in Fig (2.1b).

The simulation has been carried out by modelling an energy flux entering the system from the top-most surface that is then distributed through the whole system. With this, we expect to gain a larger temperature gradient than the ones obtained for 2D systems. The heatmap for such structure is shown in Fig. (2.7)

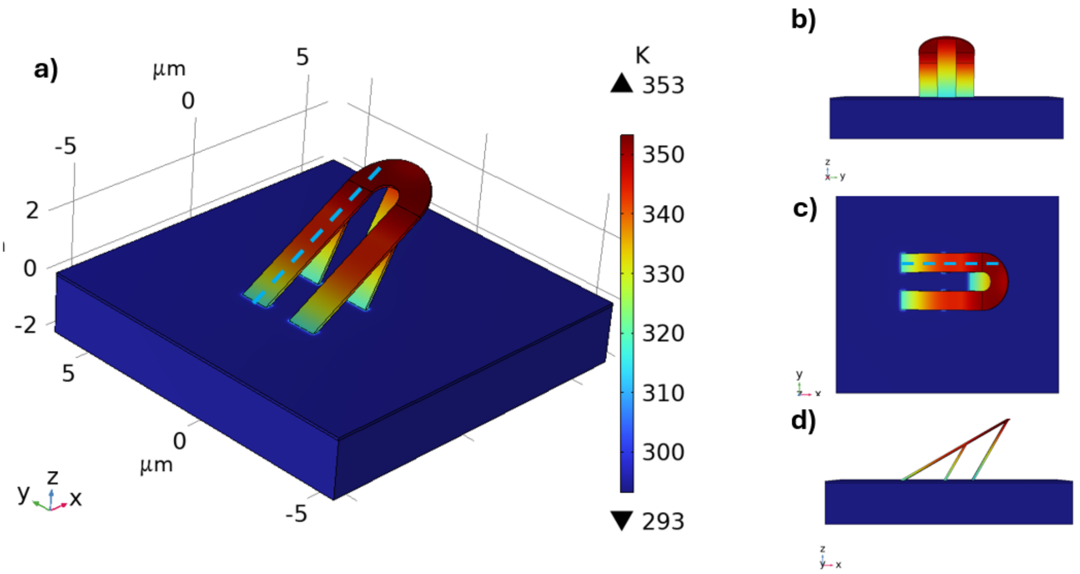

Figure 2.7: Optically heated temperature map of "horseshoe" 3D structure. Additional figures (b), (c), (d) have been included to have a more complete view of the structure in its entirety.

A line along one of the ramps has been selected to track the variation of temperature and obtain the precise gradient, shown in Fig. (2.8).

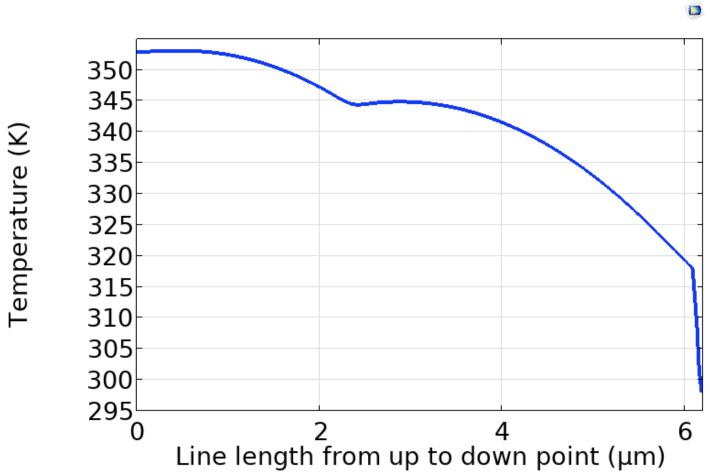

Figure 2.8: Temperature variation along the line drawn in Fig. 2.7. In the x axis, 0 represents the upper most point, and the end point of the line is located at around $6\mu m$ from there.

The measured temperature gradient in this region is approximately 10 K/μm, which is about an order of magnitude larger than the gradients obtained in the 2D simulations presented earlier. It is important to note that only about one-tenth of the laser beam's total power (around 0.3 mW) is absorbed by the device due to its smaller area compared to the focused beam, whereas the power injected into the heater in the 2D simulations is about 1 W, four orders of magnitude higher. This comparison highlights that 3D nanostructures are significantly more efficient at generating thermal gradients and, additionally, laser heating does not produce any Oersted fields making the study simpler.

Chapter 3

MuMAX3 simulations

The collective state of a system of many spins is expressed, macroscopically, through the quantity known as magnetization (M[A/m]). The total magnetization of a system is computed by integrating the magnetic state of each of the individual spins in all the system's volume (see Equation (3.1)), where $m(r, t)$ is the normalized vector field that represents the state of each spin for a given moment t.

$$M(t) = M_s \int_V m(r, t) d^3 r \tag{3.1}$$

For large systems on the order of hundreds of nanometers to a few micrometers, atomistic spin dynamics become inadequate due to their high computational cost and time requirements. At this scale, micromagnetism is more suitable for studying magnetization dynamics. MuMAX3 [34] is a simulation tool for micromagnetism. It works by modelling the state and evolution of a system of individual spins, influenced both by internal (such as exchange effects, and magnetic anisotropy) and external factors (including electric currents and external magnetic fields). It does this by using the Landau-Lifshitz-Gilbert (LLG) equation (3.2), that describes magnetization dynamics at microscopic scale.

$$\frac{d}{dt} m(r, t) = \dot{m} = -\frac{\gamma}{1+\alpha^2}\Big(m \times H_{eff} + \alpha m \times (m \times H_{eff})\Big) \tag{3.2}$$

Where γ is the gyromagnetic ratio ($1.76 \cdot 10^{11}$ rad/s) and α is the damping parameter (adimensional). This last parameter is essential as it accounts for the system's "flexibility" when accepting domain deformations. Lastly, H_{eff} (the effective field) is a combination of the external magnetic field, the demagnetizing field, and internal magnetic interactions that arise from quantum effects of the system, which, as explained before, depends on the present interactions, both internal and external.

Energetically speaking, every system tends towards stability. The time evolution of a system is driven by this tendency and the reported changes e.g. motion, deformation or nucleation of new magnetic textures, constitute steps directed to the achievement of a stable (or metastable) state of minimal energy. The effective field used in the LLG equation (3.3) is obtained from the energy functional described in (3.4) and accounts for all interactions present in the dynamics landscape of the system. It is possible thus to include other sources of effective magnetic field such as spin polarized currents to study its effects on the local and global magnetic state of a system.

$$H_{eff} = -\frac{1}{\mu_0 M_s}\frac{\delta E}{\delta m} \tag{3.3}$$

$$E[m,t] = \int_V \{A(\nabla m)^2 - \mu_0 M H_{ext} - \frac{\mu_0}{2} M H_{demag} + H_{DMI} + H_{anis} + ...\} d^3 r \tag{3.4}$$

Where the terms of the energy functional represent (from left to right):

- The exchange energy
- The associated energy to an external applied magnetic field
- The demagnetizing field energy
- The interfacial DMI energy, as shown in the introduction, in equation 1.1
- The anisotropy energy

In this section we show the results of a series of micromagnetic simulations where some of the input parameters come from the data extracted from thermal and field gradients (see 2).

The objective is to analyze the motion of Skyrmions in Pt/Co/Al and Ta/CoFeB/MgO multilayers exhibiting out-of-plane magnetic anisotropy. However, due to the absence of specialized hardware required to run fully detailed simulations, we will focus on a simplified system and consider only the Pt/Co/Al trilayer. The results presented in the previous section regarding temperature gradients and Oersted fields are incorporated into this analysis to simulate the Skyrmion properties and motion. The influence of temperature is significant, as temperature gradients cause variations in saturation magnetization, uniaxial anisotropy, exchange stiffness and DMI strength, among others, as reported in various studies [13, 16]. Their dependences with temperature are shown in Equations (3.5), (3.6), (3.7), (3.8) [16, 35].

$$M_{sat}(T) = M_{sat}(0)\Big(1 - \frac{T}{T_c}\Big)^{1.5} \tag{3.5}$$

$$Ku_1(T) = Ku_1(0)\Big(1 - \frac{T}{T_c}\Big)^{3} \tag{3.6}$$

$$A_{ex}(T) = A_{ex}(0)\Big(1 - \frac{T}{T_c}\Big)^{1.7} \tag{3.7}$$

$$DMI(T) = DMI(0)\Big(1 - \frac{T}{T_c}\Big)^{1.7} \tag{3.8}$$

Where $M_{sat}(0)$, $Ku_1(0)$, $A_{ex}(0)$, $DMI(0)$ are the values of the properties at 0K.

Methodology

We model a 2D layer of cobalt where a temperature gradient is defined according to the results obtained in chapter 2 for all structures. In all the cases the simulation was carried out using a stripe of 256x48 nm. The specific magnetic and geometric parameters for the simulations are shown in Table 3.1

Parameter	Value
Number of cells: Nx x Ny x Nz	$256 \times 48 \times 1$
Cell volume = lx x ly x lz (nm^3)	$252 \times 48 \times 1$
Damping (α)	0.05
Anisotropy direction	OOP (0,0,1)
Periodic boundary conditions	(5,0,0)
DMI (0) (J/m^2)	$2 \cdot 10^{-3}$
Aex (0) (J/m)	$1.1 \cdot 10^{-11}$
Ms (0) (A/m)	10^6
Ku1 (0) (J/m^3)	$1.2 \cdot 10^6$

Tabla 3.1: Parameters used in the MuMAX3 simulations for skyrmion motion.

After setting the initial values for the cobalt film and finding a relaxed state with Skyrmions in the system, we proceed with establishing the temperature gradients based on the results obtained before.

To emulate the gradient the system is divided in N regions in the x axis. For simplicity, the gradients are taken as linear. The temperature is then evaluated in each of the N regions, and then used to compute the exchange stiffness, DMI strength, anisotropy and saturation magnetization in them. We abstained from including thermal fluctuations, since thermal noise disturbs the simulation significantly, to the point of annihilating the Skyrmions. This poses difficulties to detect and measure the motion. These structures have been observed as stable under these conditions experimentally [36, 37] allowing us to make the assumption that disturbance due to this noise source can be neglected from our model.

Before simulating the Skyrmion motion, we first pre-nucleate a Skyrmion in the thin film. The temperature is set at 350K and the applied field at $B_z = +20mT$ [17]. This is done for both 2D and 3D. We then appropriately apply the thermal gradients by adjusting the values of the magnetic parameters considering the temperature at each point including a $\nabla T = -6K/\mu m$ for the 2D devices and a$\nabla T = -10K/\mu m$ for the 3D ones.

Results

As the objective is to understand the effect of thermal gradients on the motion of Skyrmions, here we present the behavior of Skyrmions under two different temperature gradients. Since Oersted field distributions have also been obtained, I use them to examine the influence of a field gradient on Skyrmion motion by comparing systems with and without the field, while keeping the temperature gradient constant.

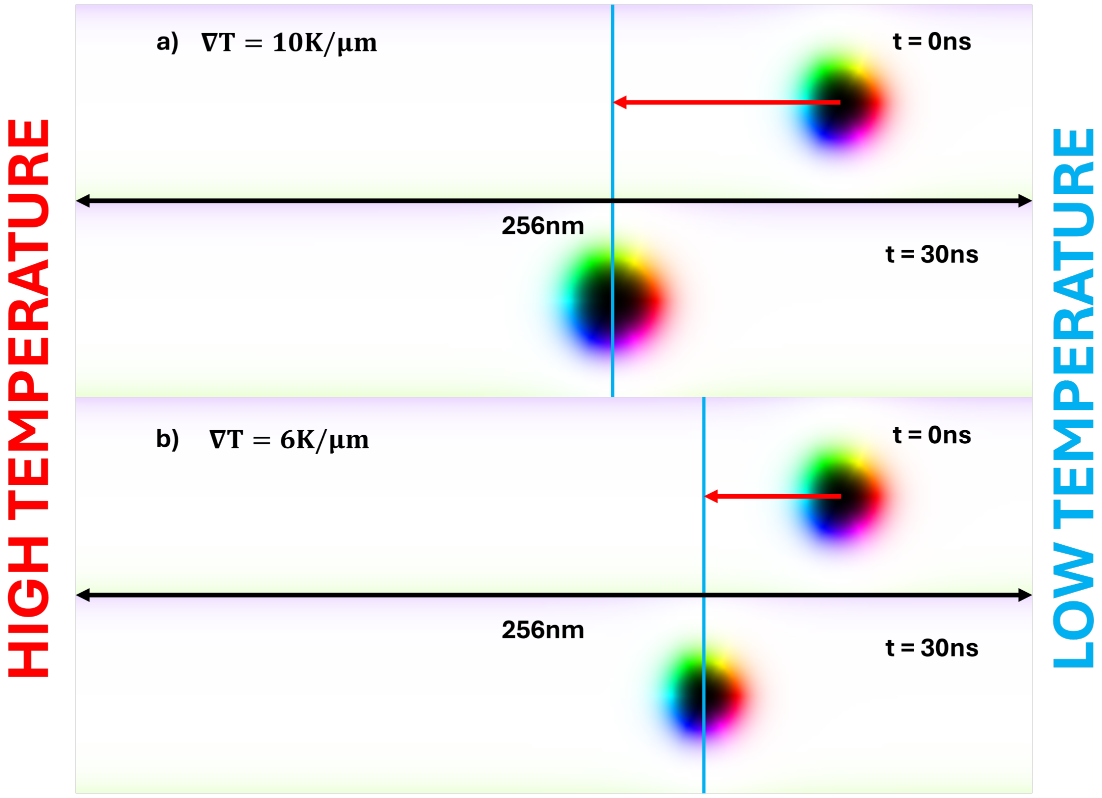

Figure 3.1: Diagram showcasing the difference in traveled length (in 30ns) for two situations, both with no out of plane field components, but with different gradients; (a) under a gradient of 10K/μm. $v_{avg} = 2.033 \pm 0.004$ m/s; (b) under a gradient of 6K/μm. $v_{avg} = 1.223 \pm 0.001$ m/s.

The simulations aim to mirror the reality as closely as possible. That is why the high temperature region always corresponds to the maximum temperature reported in the systems where we obtained these gradients. In Fig. (3.1a) the maximum temperature is 353 K whereas in Fig. (3.1b) the maximum corresponds to the maximum temperature in the SSC system gradient, 330 K.

The results show that the exposure of the sample to higher temperature gradients causes an increase in the average speed of the Skyrmions which consistently travel towards the hot region. By increasing the thermal gradient from 6 to 10 K/μm we obtain an increase in the average Skyrmion velocity of 60%. In this case, the displacement of Skyrmions toward the hot regions is driven solely by entropic torques, even though a more realistic scenario should include as well other terms such as thermally induced magnon and spin currents caused by temperature gradients[13, 16, 38, 39]. These terms however are out of the scope of this work since they require atomistic simulations to estimate more precisely the magnetic parameters. Magnonic torques require the addition of thermal spin waves generated by a stochastic thermal field in the LLG equation and thermal spin currents require an extensive material characterization to know the real damping and field-like torques in the multilayer as well as the thermal spin current generation. We thus focus here only in entropic torques, i.e. we reflect temperature changes in the material parameters, (whose dependencies have been shown previously in Equations (3.5) - (3.8)).

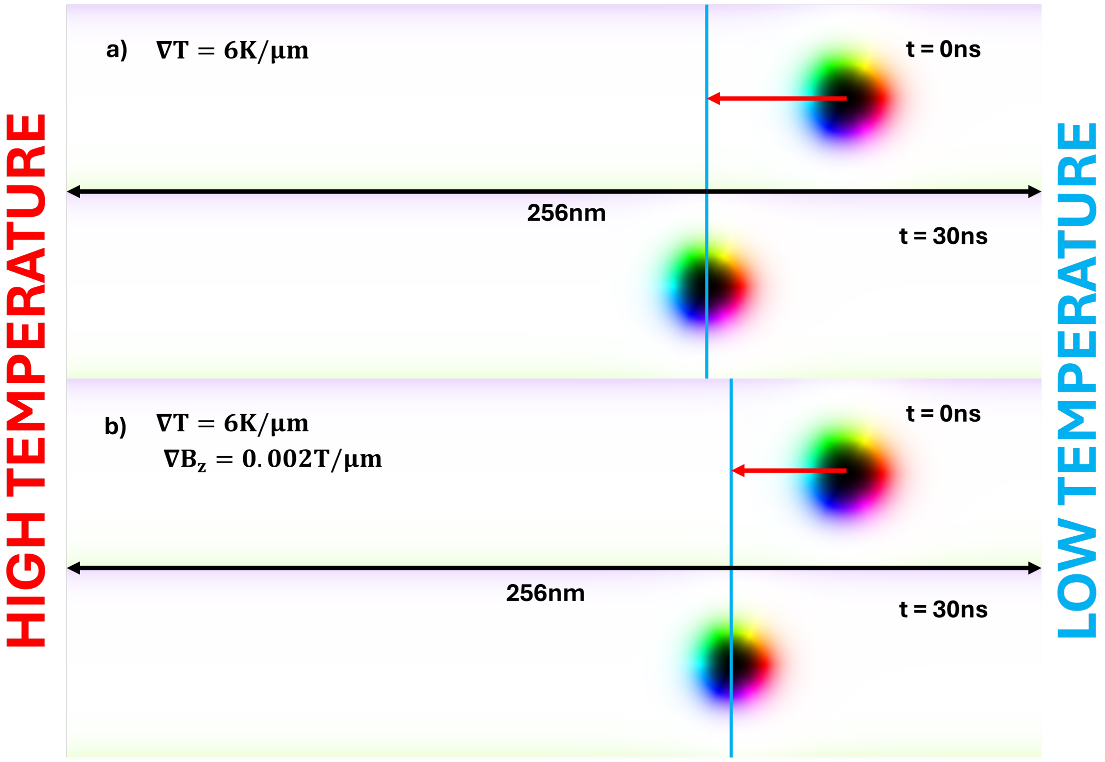

Figure 3.2: Diagram showcasing the difference in traveled length (in 30ns) for two racetracks under the same temperature gradient of 6K/μm but; (a) in abscence of field gradient $v_{avg} = 1.233 \pm 0.001$ m/s; (b) under an Oersted field gradient of 2mT/μm. $v_{avg} = 1.013 \pm 0.004$ m/s.

The effect on motion of the Oersted field gradient can be visualized in Fig. (3.2) where the traveled distance of the Skyrmion under the effect of Oersted field is slightly lower than in its absence. The existence of a field in the direction of anisotropy causes magnetic moments to be more "rigid" and less prone to accept the motion of domains, therefore slowing them down. In the case of a change of the sign of the electric current the Oersted field would flip and the speed would increase accordingly instead.

These results point to an opposite effect as observed in thermal stimulated motion experiments, where the Skyrmion travels from the higher temperature regions to the lower ones [17]. The key difference here is that with these simulations we are not modeling the contributions to motion that result in the reported movement, such as spin currents [16]. By simplifying the model, we have obtained the motion resulting from a material property gradient induced by temperature, trying to reproduce a system that resembles the real ones with the highest fidelity. The speeds reported also vary from other studies of the same nature due to this very reason [13], since instead of simulating a linear variation of properties such as uniaxial anisotropy or exchange stiffness, we have used temperature-dependent expressions for the material's parameters.

Chapter 4

Micro, nanofabrication and experimental characterization

In this chapter the focus is put on device characterization and fabrication. This has not been the central part of my work in the project. However, I was actively involved in conducting the experiments and discussions. For the sake of completeness, they are included in this chapter.

The multilayers used for the experiments follow a specific process to achieve the conformal configurations necessary to harbor Skyrmions, as explained in chapter 1. The multilayers are deposited by magnetron sputtering. Sputtering is a Physical Vapor Deposition (PVD) technique that excels at thickness control (down to sub-nm resolution), interface quality and composition. In this process, energetic ions (like Ar^+) are accelerated towards a target material. Upon impact, atoms of the target are ejected towards a substrate where the materials are deposited.

This technique allows the fabrication of multilayers where properties such as perpendicular magnetic anisotropy (PMA) and the DMI strength are enhanced so that Skyrmion nucleation becomes favorable in the system, as well as guaranteeing a certain stability of these magnetic textures. In this case, the fabricated multilayers, $[\mathrm{Ta}(5)/\mathrm{CoFeB}(0.8)/\mathrm{MgO}(1.2)]_{x3}$, were done in collaboration with TU Wien's Physics of 3D Nanomaterials group. The numbers represent the thickness of the layers in nm.

Micro and nanofabrication of devices

2D Microdevices, similar to the ones simulated in chapter 2 have been fabricated using a combination of UV lithography and ion milling.

The devices have undergone one-step lithography on the microwriter (ML3Pro), where a the multilayer is covered with a resist is exposed to UV light following the pattern that it was previously designed. The microwriter allows for geometry control without the need for masks. In this case, the substrate was coated with positive photoresist that was then exposed to the UV beam. Then, using a developer, we remove the necessary parts of the photoresist to produce the desired pattern. Finally, to remove the excess material and defects, the sample is subjected to the process of ion milling, where Argon ions are accelerated towards the sample to remove the material which was not covered by resist ensuring clean and well-defined devices. Fig. 4.1 shows a batch of devices produced using this technique. The zoomed-in version of two of the devices, showing a slightly different geometry of the heater, can be seen in Fig. 4.2.

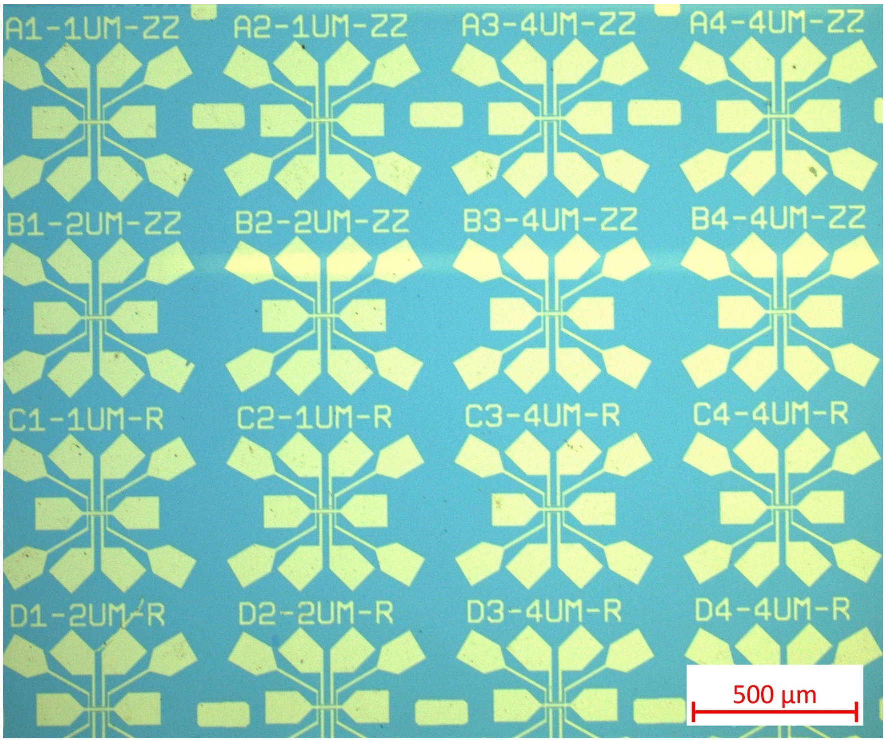

Figure 4.1: Batch of 2D microdevices fabricated by UV Lithography and ion milling. The inscriptions indicate the batch tag - width - and shape of the conductor, where ZZ refers to the ZZC setup and R to the SSC one, as shown in chapter 2.

The 3D nanostructures were fabricated by Focused Electron Beam Ion Deposition (FEBID). FEBID is a direct-write nanofabrication technique that enables the growth of 3D nanostructures with high spatial resolution using a focused electron beam to dissociate precursor gas molecules adsorbed on a substrate surface, leading to localized material deposition. It offers advantages such as resolution of a few tens of nanometers, vertical growth rates of hundreds of nanometers per second, and compatibility with a wide range of precursor materials including metallic, organic, semiconducting, magnetic, and superconducting compounds[40]. Recent developments by the group of our collaborator, Prof. Fernández-Pacheco enable the fabrication of

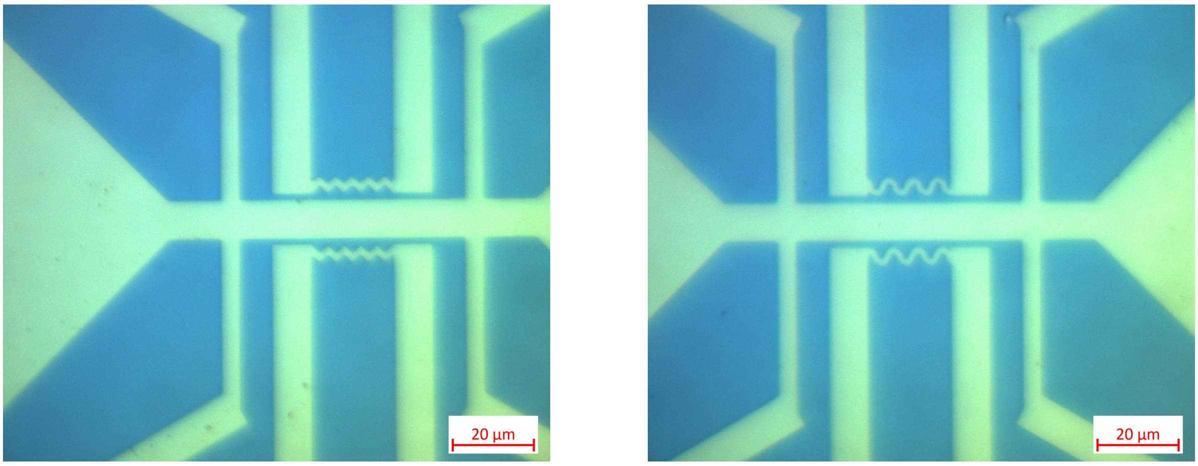

(a) (b)

Figure 4.2: (a) ZZC heater setup, labeled as ”ZZ” in Fig.(4.1). (b) SSC heater setup, labeled as ”R” in Fig.(4.1).

complex-shaped 3D nanostructures directly from standard 3D files, accounting for factors like beam-induced heating, defocusing, and gas flux anisotropy[41]. In this case, instead of constructing the whole 3D setup we wanted to analyze, we started by constructing a simplified version, consisting of only a ramp, as shown in Fig. 4.3. Here we use a Pt precursor, the most used one in FEBID. After fabrication of the ramps, we grow a similar multilayer as in the 2D devices by sputtering on top of the ramp[42] to be able to obtain Skyrmions in the 3D system, since the ramp itself is not magnetically active and cannot host them by itself.

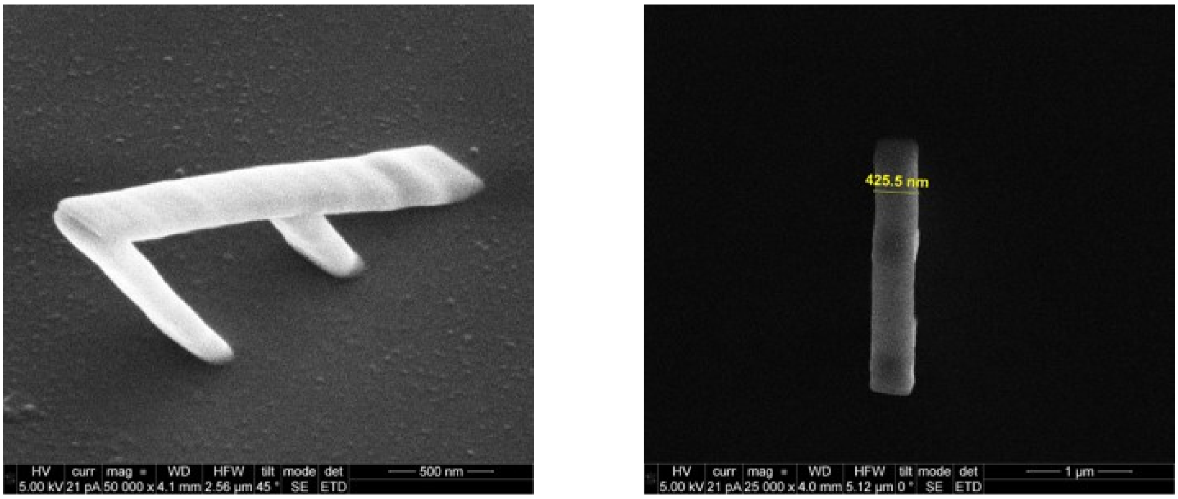

(a) (b)

Figure 4.3: (a) SEM visualization of 3D built ramp using FEBID (b) structure seen from above, showing its width (425.5nm)

Sample analysis using NanoMOKE

For the characterization of the 2D multilayer sample, we have used the NanoMOKE setup to detect the presence of Skyrmion domains in the sample. **Magneto-Optic Kerr Effect** (MOKE) technique uses polarized light that, when reflected on a magnetic material, causes a rotation of the polarization depending on the magnetization's direction in the region illuminated by the light. The NanoMOKE3 equipment includes a set of galvomirrors and lenses providing spatially resolved imaging of the Kerr rotation and reflectivity with micrometer resolution. The measurements performed with this setup have been done using the polar configuration (Fig. (4.4)) and the quadrupole magnet, allowing us to measure hysteresis loops by sweeping along the perpendicular-to-surface axis $\hat{x}$ (and therefore studying if the film exhibits PMA) as well as introducing an in-plane field offset along $\hat{y}$ to study how this affects the cycles.

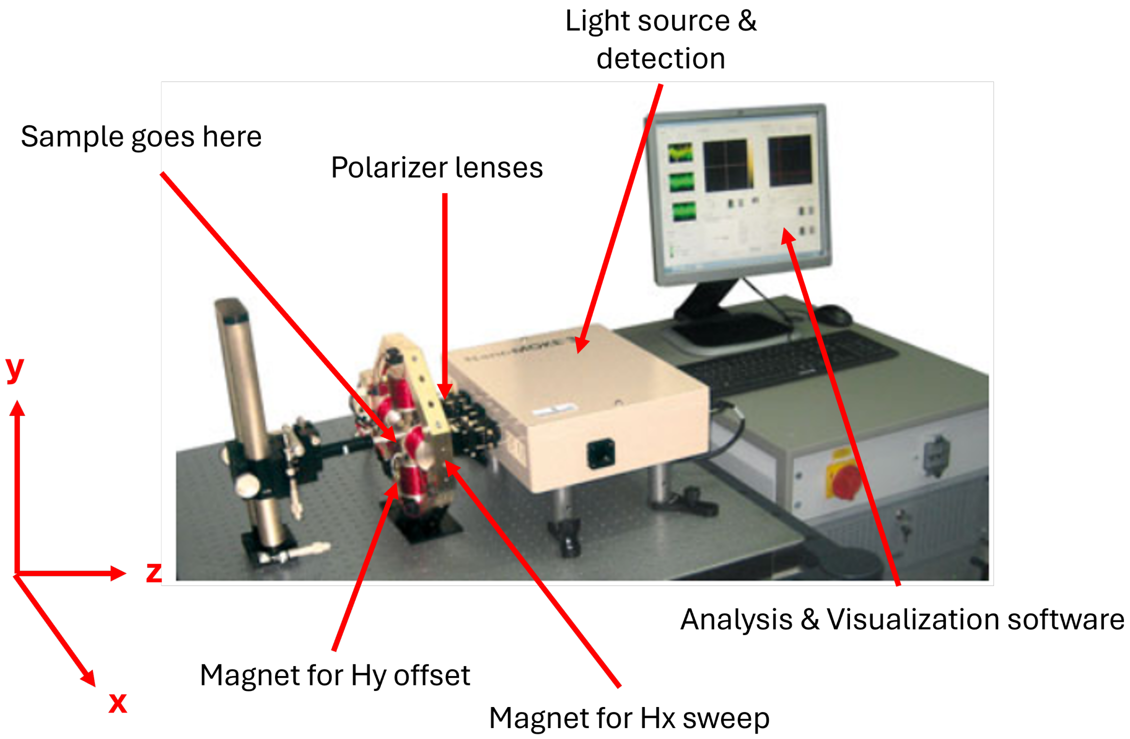

Figure 4.4: Visualization of the NanoMOKE3 setup in POLAR configuration.

Following this procedure we obtained information regarding the existence of PMA and the presence of domains. In the second case, we could not confirm accurately via imaging if the domains are Skyrmion-like, as the lateral resolution is in the order of 1 μm in optimal circumstances[43]. If Skyrmions are smaller, it becomes impossible to resolve their structure using MOKE imaging and one must resort to other techniques like synchrotron-based transmission X-ray microscopy (TXM) or X-ray magnetic circular dichroism combined with photoemission electron microscopy (XMCD-PEEM)[44]. The fact that we could not obtain clear images of Skyrmions using this setup indicates that their size is smaller than the lower resolution limit, although modifications can be done to increase it, such as using specialized objectives for ultra-high resolution.

We have used NanoMOKE and Dark Field (DFMOKE)[45] to analyze the behavior of 2D and 3D samples by sweeping across field values in the perpendicular direction to the substrate's surface while applying an in-plane bias field component. DFMOKE, an adaptation of MOKE that uses specular reflections from different planes of a 3D magnetic nanostructure to separately analyze magnetic switching in complex geometries, is particularly useful for the measurement of 3D nanostructures as conventional NanoMOKE struggles at isolating the magnetic signals of a complex 3D object.

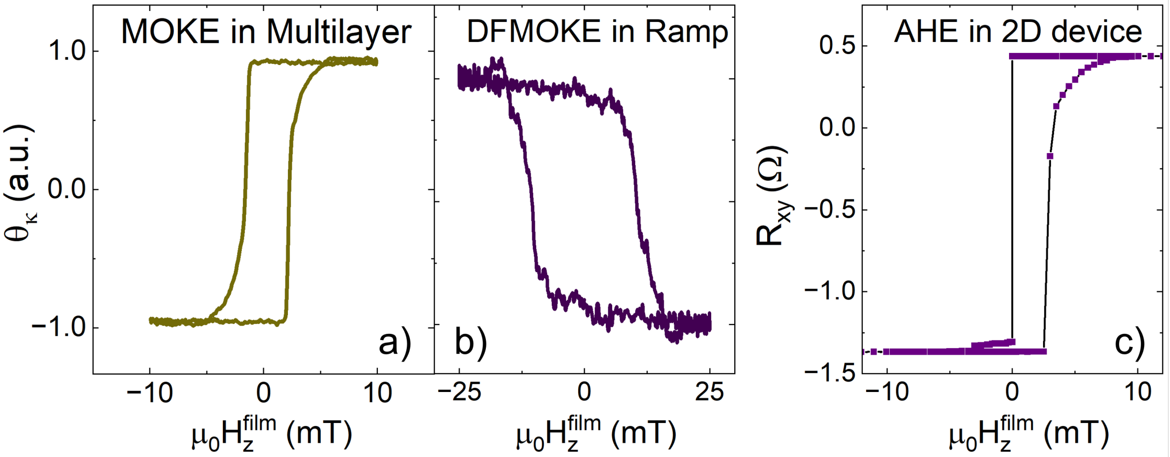

Figure 4.5: Hysteresis loops resulting from the sweeping across the x axis. Coercive field values are around ± 10 - 20 Oe. It is important to point out the fact that in MOKE measurements the quantity detected is not the magnetization state but rather the Kerr signal.

In figure 4.5 we show the hysteresis loop characterization of the $[\mathrm{MgO/CoFeB/Ta}]_{x3}$ multilayer using three different techniques, in panel a and b we show the MOKE loops taken in the full film and the DFMOKE measured on top of the 3D ramp. In panel c, we show the anomalous Hall resistance of one of the devices described in the microfabrication section.

In multilayer magnetic films hosting Skyrmions, hysteresis loops typically exhibit low coercivity, and gradual tails toward saturation. The formation and annihilation of Skyrmions and chiral domains lead to a progressive magnetization reversal, often producing plateaus or step-like features in the hysteresis loops (see e.g. [19]) as seen in figure 4.5. These signatures provide experimental evidence of topological magnetic domains stabilized by the interfacial DMI. The loop in panel b, corresponding to the multilayer grown on the ramp presents a higher coercivity, probably related with the higher roughness of the FEBID surface compared to the one grown on silicon wafers. It also shows small jumps during the reversal, consistent with domain injection due to the small size of the ramp (0.4x3 μm), comparable to the size of the expected domains.

Chapter 5

Conclusions

This master's thesis focuses on thermal and micromagnetic modeling of 2D and 3D micro- and nanostructures to generate preliminary data and support the design of better devices to study thermal nucleation and motion of Skyrmions.

The thermal COMSOL simulations reveal, as expected, that the generated thermal gradients are larger in 3D nanostructures as compared to 2D ones. I demonstrate that, in contrast to the 1 W required to generate a $6K/\mu m$, gradient in the 2D device, only a small fraction of that power—just 0.3 mW—is sufficient to produce a gradient twice as large, reaching $10K/\mu m$ in the 3D nanostructure. These results in combination with the magnetic modeling obtained via MuMAX3 for the motion of Skyrmions support the idea of a higher efficiency in motion and generation of Skyrmions in 3D nanostructures. The average velocity obtained in the 3D devices was also higher by 60% compared to the 2D ones using these parameters.

The MuMAX3 simulations give us insight on the effect of the thermal gradient on the material parameters and their influence on Skyrmion motion. It is important to keep in mind that in order to describe the whole physical picture of the system, a series of interactions/effects that have been either predicted or observed experimentally should be included, such as spin orbit and transfer torque or the influence of magnonic torques. Thermal stimulated motion of Skyrmions points to a tendency of the domains to travel from hot regions towards cold ones. Here I show that, by only considering entropic torques (changes with temperature in exchange stiffness, DMI strength, uniaxial anisotropy and saturation magnetization) into account, the Skyrmions travel on the opposite direction. Not only that, but it is also shown that the speed at which it travels increases with the imposed temperature gradient and that the presence of a magnetic field gradient in the $\hat{z}$ direction causes a reduction in such speed when traveling from the cold regions towards the hot ones. These results point out as well that the Oersted field can play a sizable (although smaller) role and devices must be design accordingly to minimize it.

In the final part of my thesis project, I actively participated in the experimental work, including the fabrication and characterization of 2D and 3D devices. The magneto-optical measurements reveal that our multilayers present a perpendicular magnetic anisotropy which is preserved even when grown on the 3D ramps. The hysteresis loops observed by optical and electrical measurements are consistent with the existence of chiral magnetic domains.

The combined results from thermal simulations, micromagnetic modeling, and experimental data highlight the strong potential of 3D nanostructures for achieving low-energy and efficient Skyrmion motion.

Chapter 6

Bibliography

[1] A. Souchet, I. BUQUICCHIO, J. COUDREAU, M. BANK, B. DURAND, M. EFOUI-HESS, L. EGAL, H. Ferreboeuf, A. GUEGUEN, H. JEANNINGROS, A. Kissi, A. BURTHE, B. NINASSI, and A. THEVE, "[the shift project] energy, climate: What virtual worlds for a sustainable real world?," 03 2024.

[2] A. V. Chumak, V. I. Vasyuchka, A. A. Serga, and B. Hillebrands, "Magnon spintronics," *Nature Physics*, vol. 11, p. 453–461, 2015.

[3] X. Wang, Y. Wang, W. Zhao, and et al., "Towards low-power computing: From devices to systems," *Nature Electronics*, vol. 5, p. 246–256, 2022.

[4] K. Jhuria, J. Hohlfeld, A. Pattabi, E. Martin, A. Y. Arriola Córdova, X. Shi, R. Lo Conte, S. Petit-Watelot, J. C. Rojas-Sanchez, G. Malinowski, S. Mangin, A. Lemaître, M. Hehn, J. Bokor, R. B. Wilson, and J. Gorchon, "Spin–orbit torque switching of a ferromagnet with picosecond electrical pulses," *Nat. Electron.*, vol. 3, pp. 680–686, Oct. 2020.

[5] M. Hoffmann, G. P. Müller, C. Melcher, and S. Blügel, "Skyrmion-antiskyrmion racetrack memory in rank-one dmi materials," *Frontiers in Physics*, vol. 9, p. 769873, 2021.

[6] N. Nagaosa and Y. Tokura, "Topological properties and dynamics of magnetic skyrmions," *Nature Nanotechnology*, vol. 8, p. 899–911, 2013.

[7] A. Fert, V. Cros, and J. Sampaio, "Skyrmions on the track," *Nat. Nanotechnol.*, vol. 8, pp. 152–156, Mar. 2013.

[8] W. Jiang, X. Zhang, G. Yu, W. Zhang, X. Wang, M. Benjamin Jungfleisch, J. E. Pearson, X. Cheng, O. Heinonen, K. L. Wang, Y. Zhou, A. Hoffmann, and S. G. E. te Velthuis, "Direct observation of the skyrmion hall effect," *Nat. Phys.*, vol. 13, pp. 162–169, Feb. 2017.

[9] I. Lima Fernandes, S. Blügel, and S. Lounis, “Spin-orbit enabled all-electrical readout of chiral spin-textures,” *Nat. Commun.*, vol. 13, p. 1576, Mar. 2022.

[10] J. Iwasaki, M. Mochizuki, and N. Nagaosa, “Current-induced skyrmion dynamics in constricted geometries,” *Nature Nanotechnology*, vol. 8, p. 742–747, 2013.

[11] T. Dohi, M. Weißenhofer, N. Kerber, F. Kammerbauer, Y. Ge, K. Raab, J. Zázvorka, M.-A. Syskaki, A. Shahee, M. Ruhwedel, T. Böttcher, P. Pirro, G. Jakob, U. Nowak, and M. Kläui, “Enhanced thermally-activated skyrmion diffusion with tunable effective gyrotropic force,” *Nat. Commun.*, vol. 14, p. 5424, Sept. 2023.

[12] K. Litzius, J. Leliaert, P. Bassirian, D. Rodrigues, S. Kromin, I. Lemesh, J. Zazvorka, K.-J. Lee, J. Mulkers, N. Kerber, D. Heinze, N. Keil, R. M. Reeve, M. Weigand, B. Van Waeyenberge, G. Schütz, K. Everschor-Sitte, G. S. D. Beach, and M. Kläui, “The role of temperature and drive current in skyrmion dynamics,” *Nat. Electron.*, vol. 3, pp. 30–36, Jan. 2020.

[13] I. R. de Assis, I. Mertig, and B. Göbel, “Skyrmion motion in magnetic anisotropy gradients: Acceleration caused by deformation,” *Phys. Rev. B.*, vol. 108, Oct. 2023.

[14] K.-Y. Kim and Y. Tserkovnyak, “Thermally driven motion of magnetic skyrmions,” *Physical Review Letters*, vol. 119, no. 4, p. 047202, 2017.

[15] J. Zázvorka, F. Jakobs, D. Heinze, N. Keil, S. Kromin, S. Jaiswal, K. Litzius, G. Jakob, D. Pinna, K. Everschor-Sitte, *et al.*, “Thermal skyrmion diffusion used in a reshuffler device,” *Nature Nanotechnology*, vol. 14, no. 7, pp. 658–661, 2019.

[16] E. Raimondo, E. Saugar, J. Barker, D. Rodrigues, A. Giordano, M. Carpentieri, W. Jiang, O. Chubykalo-Fesenko, R. Tomasello, and G. Finocchio, “Temperature-gradient-driven magnetic skyrmion motion,” *Phys. Rev. Appl.*, vol. 18, Aug. 2022.

[17] Z. Wang, M. Guo, H.-A. Zhou, L. Zhao, T. Xu, R. Tomasello, H. Bai, Y. Dong, S.-G. Je, W. Chao, H.-S. Han, S. Lee, K.-S. Lee, Y. Yao, W. Han, C. Song, H. Wu, M. Carpentieri, G. Finocchio, M.-Y. Im, S.-Z. Lin, and W. Jiang, “Thermal generation, manipulation and thermoelectric detection of skyrmions,” *Nature Electronics*, vol. 3, p. 672–679, Oct. 2020.

[18] W. Kang, Y. Huang, C. Zheng, W. Lv, N. Lei, Y. Zhang, X. Zhang, Y. Zhou, and W. Zhao, “Voltage controlled magnetic skyrmion motion for racetrack memory,” *Sci. Rep.*, vol. 6, p. 23164, Mar. 2016.

[19] S. Woo, K. Litzius, B. Krüger, M.-Y. Im, L. Caretta, K. Richter, M. Mann, A. Krone, R. M. Reeve, M. Weigand, P. Agrawal, I. Lemesh, M.-A. Mawass, P. Fischer, M. Kläui, and G. S. D. Beach, “Observation of room-temperature magnetic skyrmions and their current-driven dynamics in ultrathin metallic ferromagnets,” *Nat. Mater.*, vol. 15, pp. 501–506, May 2016.

[20] A. Fert, N. Reyren, and V. Cros, “Magnetic skyrmions: advances in physics and potential applications,” *Nature Reviews Materials*, vol. 2, p. 17031, 2017.

[21] T. H. R. Skyrme, “A unified field theory of mesons and baryons,” *Nuclear Physics*, vol. 31, pp. 556–569, 1962.

[22] F. Hellman, A. Hoffmann, Y. Tserkovnyak, G. S. Beach, E. E. Fullerton, C. Leighton, A. H. MacDonald, D. C. Ralph, D. A. Arena, H. A. Dürr, *et al.*, “Interface-induced phenomena in magnetism,” *Reviews of modern physics*, vol. 89, no. 2, p. 025006, 2017.

[23] E. Burgos-Parra, Y. Sassi, W. Legrand, F. Ajejas, C. Léveillé, P. Gargiani, M. Valvidares, N. Reyren, V. Cros, N. Jaouen, *et al.*, “Probing of three-dimensional spin textures in multilayers by field dependent x-ray resonant magnetic scattering,” *Scientific Reports*, vol. 13, no. 1, p. 11711, 2023.

[24] K.-W. Kim, J.-M. Han, and K.-J. Lee, “Spin wave driven skyrmions in a bipartite antiferromagnetic lattice,” *Physical Review B*, vol. 109, no. 1, p. 014435, 2024.

[25] N. Nagaosa, J. Sinova, S. Onoda, A. H. MacDonald, and N. P. Ong, “Anomalous hall effect,” *Reviews of modern physics*, vol. 82, no. 2, pp. 1539–1592, 2010.

[26] R. Ramos, M. H. Aguirre, A. Anadón, J. Blasco, I. Lucas, K. Uchida, P. A. Algarabel, L. Morellón, E. Saitoh, and M. R. Ibarra, “Anomalous nernst effect of fe_3o_4 single crystal,” *Phys. Rev. B*, vol. 90, p. 054422, Aug 2014.

[27] S. Qiu, J. Zeng, X. Han, and J. Liu, “On-chip skyrmion synapse regulated by oersted field,” *AIP Advances*, vol. 14, p. 035105, 03 2024.

[28] X. Zhang, Y. Zhou, M. Ezawa, G. P. Zhao, and W. Zhao, “Magnetic skyrmion transistor: skyrmion motion in a voltage-gated nanotrack,” *Scientific Reports*, vol. 5, p. 11369, 2015.

[29] L. Berges, E. Haltz, S. Panigrahy, S. Mallick, R. Weil, S. Rohart, A. Mougin, and J. Sampaio, “Size-dependent mobility of skyrmions beyond pinning in ferrimagnetic GdCo thin films,” *Phys. Rev. B.*, vol. 106, Oct. 2022.

[30] W. J. et al., “Blowing magnetic skyrmion bubbles,” *Science*, vol. 349, pp. 283–286, 2015.

[31] A. Kuprava and M. Huth, “Fast and efficient simulation of the febid process with thermal effects,” *Nanomaterials*, vol. 13, no. 5, p. 858, 2023.

[32] T. Piasecki, K. Kwoka, E. Gacka, P. Kunicki, and T. Gotszalk, “Electrical, thermal and noise properties of platinum-carbon free-standing nanowires designed as nanoscale resistive thermal devices,” *Nanotechnology*, vol. 35, no. 11, p. 115502, 2023.

[33] J. Zheng, Z. Li, M. Zhang, and T. Zhang, “Enhancing reflectivity of tantalum oxide coatings through plasma spraying and annealing techniques,” *Materials Letters*, vol. 378, p. 137585, 2025.

[34] A. Vansteenkiste, J. Leliaert, M. Dvornik, M. Helsen, F. Garcia-Sanchez, and B. Van Waeyenberge, “The design and verification of mumax3,” *AIP advances*, vol. 4, no. 10, 2014.

[35] Y. Zhou, R. Mansell, S. Valencia, F. Kronast, and S. van Dijken, “Temperature dependence of the dzyaloshinskii–moriya interaction in ultrathin films,” *Physical Review B*, vol. 101, no. 5, p. 054433, 2020.

[36] W. Legrand, D. Maccariello, N. Reyren, K. Garcia, C. Moutafis, C. Moreau-Luchaire, S. Collin, K. Bouzehouane, V. Cros, and A. Fert, “Room-Temperature Current-Induced generation and motion of sub-100 nm skyrmions,” *Nano Lett.*, vol. 17, pp. 2703–2712, Apr. 2017.

[37] P. Olleros-Rodríguez, M. Strungaru, S. Ruta, P.-I. Gavriloaea, A. Gudín, P. Perna, R. Chantrell, and O. Chubykalo-Fesenko, “Non-equilibrium heating path for the laser-induced nucleation of metastable skyrmion lattices,” *Nanoscale*, vol. 14, pp. 15701–15712, Nov. 2022.

[38] G.-M. Choi, B.-C. Min, K.-J. Lee, and D. G. Cahill, “Spin current generated by thermally driven ultrafast demagnetization,” *Nature communications*, vol. 5, no. 1, p. 4334, 2014.

[39] M. Weiler, M. Althammer, F. D. Czeschka, H. Huebl, M. S. Wagner, M. Opel, I.-M. Imort, G. Reiss, A. Thomas, R. Gross, and S. T. B. Goennenwein, “Local charge and spin currents in magnetothermal landscapes,” *Phys. Rev. Lett.*, vol. 108, p. 106602, Mar 2012.

[40] J. De Teresa, A. Fernández-Pacheco, R. Córdoba, L. Serrano-Ramón, S. Sangiao, and M. R. Ibarra, “Review of magnetic nanostructures grown by focused electron beam induced deposition (febid),” *Journal of Physics D: Applied Physics*, vol. 49, no. 24, p. 243003, 2016.

[41] L. Skoric, D. Sanz-Hernández, F. Meng, C. Donnelly, S. Merino-Aceituno, and A. Fernández-Pacheco, “Layer-by-layer growth of complex-shaped three-dimensional nanostructures with focused electron beams,” *Nano Letters*, vol. 20, no. 1, pp. 184–191, 2019.

[42] F. Meng, C. Donnelly, L. Skoric, A. Hierro-Rodriguez, J.-w. Liao, and A. Fernández-Pacheco, “Fabrication of a 3d nanomagnetic circuit with multi-layered materials for applications in spintronics,” *Micromachines*, vol. 12, no. 8, p. 859, 2021.

[43] Quantum Design, *NanoMOKE3 Specification Document, Version 3.2.* Quantum Design, 2024. `https://www.qd-latam.com/downloads/69/NanoMOKE3-specification-document-v3.2.pdf`.

[44] K. Litzius, I. Lemesh, B. Krüger, P. Bassirian, L. Caretta, K. Richter, F. Büttner, K. Sato, O. A. Tretiakov, J. Förster, R. M. Reeve, M. Weigand, I. Bykova, H. Stoll, G. Schütz, G. S. D. Beach, and M. Kläui, “Skyrmion hall effect revealed by direct time-resolved x-ray microscopy,” *Nat. Phys.*, vol. 13, pp. 170–175, Feb. 2017.

[45] D. Sanz-Hernández, L. Skoric, M. Ángel Cascales-Sandoval, and A. Fernández-Pacheco, “Probing 3d magnetic nanostructures by dark-field magneto-optical kerr effect,” *Journal of Applied Physics*, vol. 133, no. 4, p. 043901, 2023.

[46] Y. Wang, T. Kitamura, J. Wang, H. Hirakata, and T. Shimada, “Mechanical acceleration and control of the thermal motion of a magnetic skyrmion,” *Physical Review Applied*, vol. 18, no. 1, p. 014049, 2022.

[47] S. Qiu, J. Zeng, X. Han, and J. Liu, “On-chip skyrmion synapse regulated by oersted field,” *AIP Advances*, vol. 14, no. 3, p. 035105, 2024.

List of figures

List of tables